

Thermal Rectification through Vacuum

Clayton R. Otey,^{1,*} Wah Tung Lau (留華東),² and Shanhui Fan (范汕澗)^{2,†}

¹*Applied Physics Department, Stanford University, Stanford California, 94305, USA*

²*Department of Electrical Engineering, Ginzton Laboratory, Stanford University, Stanford California, 94305, USA*
(Received 16 November 2009; published 13 April 2010)

We propose a mechanism for photon mediated thermal rectification through vacuum relying only on the temperature dependence of electromagnetic resonances. We also propose an example implementation consisting of two polytypes of silicon carbide, which exploits the interaction of temperature dependent surface phonon polaritons to achieve significant rectification.

DOI: 10.1103/PhysRevLett.104.154301

PACS numbers: 44.40.+a, 71.36.+c

A thermal rectifier is a two terminal device with a thermal conductance that depends on the direction of heat flow. These devices allow for novel thermal management capabilities, and have possible applications in nano-scale heat regulation [1]. For this reason, there has been considerable recent interest in realizing thermal rectification. Experimentally, thermal rectification has been observed in carbon nanotube structures [2], in quantum dots [3], and in bulk oxide materials [4]. There exist other theoretical models for thermal rectifiers relying on various mechanisms, including nonlinear lattice vibrations [5,6] and nonlinear electron gas dispersion in conductors [7]. In all of these approaches, thermal rectification is a result of nonlinearity in the heat conducting channels between the terminals.

In this Letter, we propose a photon based thermal rectification scheme, in which all thermal energy transfer takes place through vacuum. Existing rectification schemes focus on regulating phonon and electron mediated thermal transfer. However, photons are also an important carrier of thermal energy. Developing a photon based rectification scheme is therefore of general importance. Moreover, since the nonlinearities in photonic systems are typically much weaker than those in phononic and electronic systems, study of photon based schemes can provide new insights into the physics of thermal rectification in general.

In our scheme, the heat conducting channels themselves have no nonlinearity. Instead, the only nonlinearity required is the temperature dependence of electromagnetic resonances that are connected to these channels. This type of nonlinearity should be readily available in a large number of material systems, since in general the refractive index of any material is temperature dependent.

We begin by considering two different bodies, labeled 1 and 2, held at fixed temperatures and separated by vacuum. In what we refer to as the forward temperature biased scenario, body 1 is held at temperature T_h and body 2 is held at T_l , with $T_h > T_l$. In the reverse temperature biased scenario, the temperatures of the bodies are swapped. We say that there is thermal rectification if the magnitudes of thermal energy transfer in the two scenarios are different.

Our central observation is that if the spectral characteristics of the two bodies have different temperature dependence, then thermal rectification, however small, is the rule rather than the exception. The rectification effect can be enhanced if the spectral characteristics of the two bodies are relatively narrow band resonances, and there is a significant difference in the temperature dependence of these two resonances. These two conditions form the basis for our rectification scheme.

An ideal rectification scheme is illustrated in Fig. 1, which contrasts the forward temperature biased (labeled *F*) and reverse temperature biased (labeled *R*) scenarios for

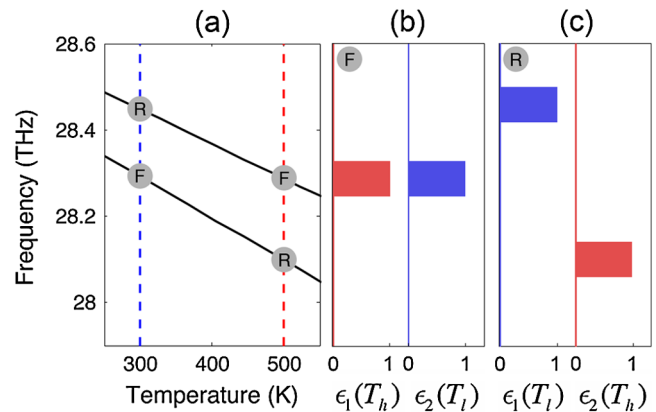


FIG. 1 (color online). (a) The black lines denote the temperature dependence of two different electromagnetic resonances, one localized around body 1 and the other around body 2. The vertical dashed lines mark the operating temperatures $T_l \sim 300$ K and $T_h \sim 500$ K. The circles with an F mark the operating points in the forward temperature biased scenario, and the circles with an R mark the operating points in the reverse temperature biased scenario. For concreteness, the two curves shown here are the surface phonon polariton frequencies of two polytypes of silicon carbide. The upper curve corresponds to SiC-3C and the lower curve corresponds to SiC-6H with the extraordinary axis normal to the surface. (b) The (overlapping) narrow-band spectral emissivities of the materials in the forward temperature biased scenario. (c) The (nonoverlapping) narrow-band spectral emissivities of the materials in the reverse temperature biased scenario. Note that (b) and (c) are hypothetical spectra.

a hypothetical pair of distantly separated bodies with particular temperature dependent resonances in their spectral emissivities. We suppose that in the forward biased case, the resonances are spectrally aligned, so that strong electromagnetic coupling between the resonances can occur. We further suppose that in the reverse biased case the resonances are spectrally separated, so that the resonances are weakly coupled. Figure 1(a) depicts a temperature dependence for the resonant frequencies of the spectral emissivities $\epsilon_{1,2}(T)$ of bodies 1 and 2, which meets these criteria. These spectral emissivities are idealized as perfect step functions, with unity emissivity in a narrow band around the resonance, and zero emissivity outside this narrow band, as shown in Figs. 1(b) and 1(c).

In the forward biased scenario, shown in Fig. 1(b), the result would be a net transfer of thermal energy from the hot body 1 to the cold body 2, due to photons in the narrow band where the spectral emissivities overlap. In the reverse biased scenario, as shown in Fig. 1(c), there is no overlap of the spectral emissivities, and no thermal electromagnetic energy is transferred in either direction. The rectification in this example is perfect; i.e., heat will flow only in the forward temperature biased scenario.

Although we have initially formulated our scheme in the context of resonances of far field emissivity, the same conditions should apply to any resonances that mediate thermal energy transfer, provided that the heat conducting channels are linear so that the spectral overlap is solely determined by the temperature dependence of the resonances. We will now describe a coupled mode theory for this class of models, which consists of a collection of independent thermal energy transfer channels, indexed by a parameter β (which will later correspond to a transverse wave number in our particular implementation of this model). Each channel consists of two coupled lossy modes, one localized around body 1 and the other around body 2. For each mode, the loss introduces an intrinsic decay rate, which by the fluctuation-dissipation theorem also implies coupling to compensating noise sources [8].

We denote the mode amplitudes by a_1 and a_2 , the noise sources by n_1 and n_2 , the resonant frequencies (which depend on temperature) by ω_1 and ω_2 , the loss rates by γ_1 and γ_2 , and the coupling rate of the modes by κ . The β dependence and temperature dependence of these parameters are suppressed for the moment. The coupled mode equations can be written as

$$\begin{aligned}\frac{da_1}{dt} &= i\omega_1 a_1 - \gamma_1 a_1 + i\kappa a_2 + \sqrt{2\gamma_1} n_1 \\ \frac{da_2}{dt} &= i\omega_2 a_2 - \gamma_2 a_2 + i\kappa^* a_1 + \sqrt{2\gamma_2} n_2.\end{aligned}\quad (1)$$

We normalize the amplitudes so that the mode energies are given by $|a_1|^2$ and $|a_2|^2$. The net ensemble average power $\langle S \rangle$ transferred from mode 1 to mode 2 is then related to the amplitude correlation between the resonances,

$$\begin{aligned}\langle S(t) \rangle &= 2\text{Im}[\kappa \langle a_1^*(t) a_2(t) \rangle] \\ &= 2\text{Im} \left[\kappa \int_{-\infty}^{\infty} \frac{d\omega}{2\pi} \int_{-\infty}^{\infty} \frac{d\omega'}{2\pi} e^{i(\omega' - \omega)t} \langle a_1^*(\omega) a_2(\omega') \rangle \right].\end{aligned}\quad (2)$$

The frequency domain amplitude correlation can be solved for, in terms of the correlations of the thermal noise sources, using Eq. (1). In the forward biased scenario, the correlations of the noise source are [8]

$$\begin{aligned}\langle n_1(\omega) n_2^*(\omega') \rangle &= \Theta(\omega, T_h) 2\pi \delta(\omega - \omega') \\ \langle n_2(\omega) n_2^*(\omega') \rangle &= \Theta(\omega, T_l) 2\pi \delta(\omega - \omega') \\ \langle n_1(\omega) n_2^*(\omega') \rangle &= \langle n_2(\omega) n_1^*(\omega') \rangle = 0,\end{aligned}\quad (3)$$

where $\Theta(\omega, T) = \frac{\hbar\omega}{e^{\hbar\omega/k_B T} - 1}$. The result is

$$\langle S_f(t) \rangle = \int_{-\infty}^{\infty} d\omega \langle S_f(\omega) \rangle \quad (4)$$

where the spectral power (which is not the Fourier transform of $S_f(t)$) is

$$\langle S_f(\omega) \rangle = \frac{2|\kappa|^2 \gamma_1 \gamma_2}{\pi} \frac{[\Theta(\omega, T_h) - \Theta(\omega, T_l)]}{\{i[\omega - \omega_1(T_h)] + \gamma_1\} \{i[\omega - \omega_2(T_l)] + \gamma_2\} + |\kappa|^2}. \quad (5)$$

Similar results hold for $\langle S_r(\omega) \rangle$, the spectral power transfer in the reverse biased scenario. The thermal rectification can now be defined as the relative difference in the net power transfer in the two scenarios.

$$R = \frac{\sum_{\beta} \int_{-\infty}^{\infty} d\omega (\langle S_f(\beta, \omega) \rangle - \langle S_r(\beta, \omega) \rangle)}{\sum_{\beta} \int_{-\infty}^{\infty} d\omega \langle S_r(\beta, \omega) \rangle}. \quad (6)$$

From Eqs. (5) and (6), we see that this model exhibits nonzero rectification provided the temperature dependencies of ω_1 and ω_2 are different.

We are now in a position to design a thermal rectifier based on these principles, which amounts to choosing a

pair of temperature dependent electromagnetic resonances. In this work, motivated by recent experimental work on near-field thermal transfer [9,10], we propose to make use of surface phonon polariton resonances. In addition to providing the necessary narrow-band spectral features, surface polaritons greatly enhance the magnitude of near-field thermal energy flux [11].

Figures 2(a) and 2(b) show a schematic of a near-field photon mediated thermal rectifier. The system consists of one half-space of isotropic 3C polytype silicon carbide (SiC-3C) and one half-space of uniaxial 6H polytype silicon carbide (SiC-6H), separated by a vacuum gap d . The extraordinary axis is normal to the slab surfaces. SiC is

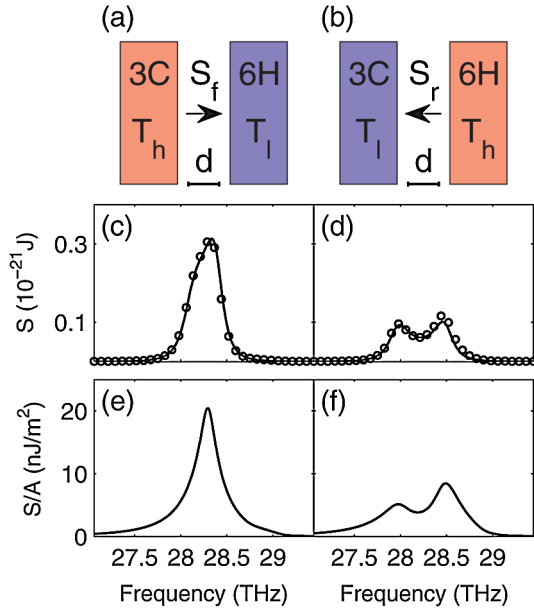


FIG. 2 (color online). Schematic of a near-field photon mediated thermal rectifier in (a) the forward, and (b) the reverse temperature biased scenarios. The device consists of a slab of SiC-3C and a slab of SiC-6H, separated by a vacuum gap d . (c), (d) The single channel spectral thermal energy flux in the two scenarios, calculated from the coupled mode model (solid line) and fluctuational electrodynamics (circles) at $\beta = 2/d$. (e), (f) The total spectral thermal energy flux in the two scenarios, calculated from fluctuational electrodynamics.

chosen because its transverse optical (TO) phonons provide clean, well studied, and relatively narrow band electromagnetic resonances in the infrared [12–14]. SiC-3C has a single TO phonon frequency, and SiC-6H has two different TO phonon frequencies, corresponding to the ordinary and extraordinary crystal axes. All of these TO phonons couple with electromagnetic waves to create phonon polaritons. Our design relies upon the difference, in

resonant frequency and the temperature dependence of the resonant frequency, between the extraordinary axis 6H and the 3C phonon polaritons.

Following [15], the thermal power transfer between the slabs can be calculated from fluctuational electrodynamics by determining the ensemble average of the Poynting vector when thermally excited sources are present in the slabs. This ensemble average can be written in terms of the correlation of the electric and magnetic fields. These fields are then written in terms of the thermal current sources and the dyadic Green functions for Maxwell's equations. The correlation of the current sources is then provided by the fluctuation-dissipation theorem. Ref. [15] deals with the case where the slabs have an isotropic dielectric tensor. In our case, where the dielectric tensor is uniaxial anisotropic, we choose the coordinate system so that the dielectric tensor is diagonal, and the fluctuation-dissipation theorem takes the form [16]

$$\langle j_k(r, \omega) j_l^*(r', \omega') \rangle = 2\Theta(\omega, T)\omega \text{Im}[\varepsilon_0 \varepsilon_{kk}(r, \omega)] \times \delta(r - r') \delta_{kl} 2\pi \delta(\omega - \omega'). \quad (7)$$

The dyadic Green functions also take a modified form in the uniaxial anisotropic case [17].

As in [15], the calculation is performed in k space. The slabs each have a transverse area A , which is assumed to be sufficiently large so that the transverse wave number β is approximately conserved in different media. Each β corresponds to an independent channel in the coupled mode model. The result of the calculation is the positive frequency spectral power transfer,

$$\langle S_f(\omega) \rangle = \sum_{\beta} S_{1 \rightarrow 2}(\beta, \omega, T_h) - S_{2 \rightarrow 1}(\beta, \omega, T_l). \quad (8)$$

In Eq. (8), $S_{1 \rightarrow 2}(\beta, \omega, T_h)$ is the spectral power absorbed in body 2 resulting from the fluctuating current in body 1, maintained at a temperature T_h ,

$$S_{1 \rightarrow 2}(\beta, \omega, T) = \frac{8}{\pi} \Theta(\omega, T) |k_{zv}|^2 \left[\frac{\text{Re}(k_{z1o}) \text{Re}(k_{z1e})}{|C_{\perp}|^2} + \frac{\text{Re}(\varepsilon_{2o}^* k_{z2e})}{2 \text{Im}(k_{z1e}) |C_P|^2} \left[|k_{z1e}|^2 \text{Im}(\varepsilon_{1o}) + \beta^2 \left| \frac{\varepsilon_{1o}}{\varepsilon_{1e}} \right|^2 \text{Im}(\varepsilon_{1e}) \right] \right], \quad (9)$$

where

$$\begin{aligned} k_{z1o} &= \sqrt{\varepsilon_{1o}(\omega/c)^2 - \beta^2}, & k_{z2o} &= \sqrt{\varepsilon_{2o}(\omega/c)^2 - \beta^2} \\ k_{zv} &= \sqrt{(\omega/c)^2 - \beta^2} & k_{z1e} &= \sqrt{\varepsilon_{1o}(\omega/c)^2 - \beta^2/\varepsilon_{1e}}, \\ & & k_{z2e} &= \sqrt{\varepsilon_{2o}(\omega/c)^2 - \beta^2/\varepsilon_{2e}} \\ C_P &= (\varepsilon_{1o} k_{zv} + k_{z1e})(\varepsilon_{2o} k_{zv} + k_{z2e}) e^{ik_{zv}d} \\ &\quad - (\varepsilon_{1o} k_{zv} - k_{z1e})(\varepsilon_{2o} k_{zv} - k_{z2e}) e^{-ik_{zv}d}, \\ C_{\perp} &= (k_{zv} + k_{z1o})(k_{zv} + k_{z2o}) e^{ik_{zv}d} \\ &\quad - (k_{zv} - k_{z1o})(k_{zv} - k_{z2o}) e^{-ik_{zv}d}. \end{aligned} \quad (10)$$

Here ε corresponds to the dielectric constant, and the o and

e subscripts correspond to the ordinary and extraordinary axes, respectively. The energy flux $S_{2 \rightarrow 1}(\beta, \omega, T_l)$, and the reverse temperature biased energy flux are calculated in a similar fashion.

We consider first the single channel case, analyzing the summand in Eq. (8) for $\beta = 2/d$, $d = 100$ nm, $T_l = 300$ K, and $T_h = 600$ K, and comparing to the coupled mode theory of Eq. (5). The channel with $\beta = 2/d$ provides nearly maximum thermal transfer between the slabs. The single channel spectral thermal energy flux, as calculated from fluctuational electrodynamics and from coupled mode theory, is plotted for the forward biased scenario in Fig. 2(c), and for the reversed biased scenario in Fig. 2(d). The coupled mode model parameters ω_1 and ω_2 used to

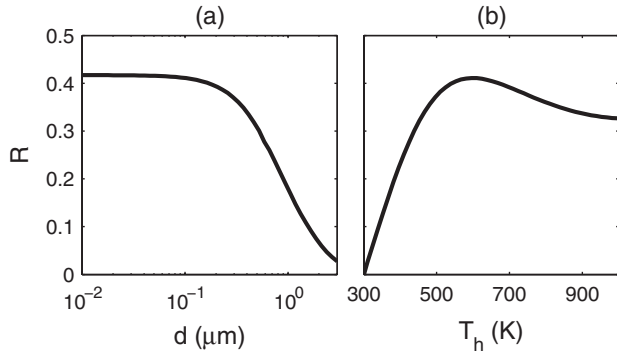


FIG. 3. (a) The rectification as a function of separation d for fixed $T_h = 600$ K, $T_l = 300$ K. (b) The rectification as function of T_h for fixed $T_l = 300$ K, $d = 100$ nm.

construct Fig. 2 are determined from the single slab surface polariton dispersion relations. The temperature dependence of ω_1 and ω_2 is shown in Fig. 1(a). The remainder of the coupled mode parameters γ_1 , γ_2 , and κ are determined from a best fit to the fluctuational electrodynamics calculation. The values for these parameters are $\kappa = 0.94 \times 10^{12} \text{ s}^{-1}$, $\gamma_1 = 1.3 \times 10^{12} \text{ s}^{-1}$, and $\gamma_2 = 0.52 \times 10^{12} \text{ s}^{-1}$ in the forward biased scenario, and $\kappa = 0.94 \times 10^{12} \text{ s}^{-1}$, $\gamma_1 = 0.81 \times 10^{12} \text{ s}^{-1}$, and $\gamma_2 = 0.87 \times 10^{12} \text{ s}^{-1}$ in the reverse biased scenario.

The two calculations yield nearly identical thermal energy flux spectra for this single channel. In the forward biased scenario, there is a single large peak present near the single slab surface polariton frequency, which is the same for both materials in this scenario. In the reversed biased scenario, there are two smaller peaks corresponding roughly to the surface polariton frequencies of the two slabs (with an additional splitting due to mode coupling). The marked difference between the spectra in the two scenarios results in rectification.

The rectification effect is mostly due to channels with $\beta \approx 2/d$. For very small β , the mode coupling rate κ becomes so large compared to the decay rates $\gamma_{1,2}$ that the peaks split markedly even when the single slab surface polariton frequencies match. For channels with very large β , the magnitude of thermal power transfer is very small. For both cases the contribution to the rectification is negligible.

The total spectral thermal energy flux in the two scenarios, calculated from fluctuational electrodynamics and summed over all β , is shown in Figs. 2(e) and 2(f). The qualitative behavior is indeed similar to the single channel case. Finally, by integrating over ω , we calculate a rectification $R = 0.41$ for this parameter set.

As seen in Fig. 3(a), the rectification falls off rapidly roughly for d larger than $1 \mu\text{m}$, due to the exponential

decay of the surface polaritons, which highlights the near-field nature of this particular implementation of our scheme. Figure 3(b) shows the rectification as a function of T_h for a fixed $T_l = 300$ K. The maximum rectification $R = 0.41$ occurs when $T_h \sim 600$ K. Note that this T_h deviates from the temperature ~ 500 K for which the single slab surface polariton frequencies are equal in the forward biased scenario. This deviation is consistent with Eqs. (5) and (6), however.

We conclude by noting that, with a nominal value $d = 100$ nm, a slab thickness of $10 \mu\text{m}$, and transverse slab dimensions $>10 \mu\text{m}$, the macroscopic electromagnetic theory and the assumption of infinite slab dimensions we employed are quite valid, and the effects of thermal expansion are negligible. Furthermore, the separation $d = 100$ nm is technically reasonable in light of recent thermal transfer experiments [9,10], and though our calculations assume a plane-plane geometry for simplicity, the same principles should apply to the sphere-plane geometry used in these experiments.

This work is supported in part by an AFOSR-MURI program (Grant No. FA9550-08-1-0407).

*otey@stanford.edu

†shanhui@stanford.edu

- [1] L. Wang and B. Li, *Phys. World* **21**, 27 (2008).
- [2] C.W. Chang *et al.*, *Science* **314**, 1121 (2006).
- [3] R. Scheibner *et al.*, *New J. Phys.* **10**, 083016 (2008).
- [4] W. Kobayashi, Y. Teraoka, and L. Terasaki, *Appl. Phys. Lett.* **95**, 171905 (2009).
- [5] M. Terraneo, M. Peyrard, and G. Casati, *Phys. Rev. Lett.* **88**, 094302 (2002).
- [6] B. Li, L. Wang, and G. Casati, *Phys. Rev. Lett.* **93**, 184301 (2004).
- [7] D. Segal, *Phys. Rev. Lett.* **100**, 105901 (2008).
- [8] H. Haus, *Electromagnetic Noise and Quantum Optical Measurements* (Springer-Verlag, Berlin, 2000), p. 143. Our convention for the inverse Fourier Transform differs by a factor of 2π .
- [9] S. Shen, A. Narayanaswamy, and G. Chen, *Nano Lett.* **9**, 2909 (2009).
- [10] E. Rousseau *et al.*, *Nature Photonics* **3**, 514 (2009).
- [11] A. Shchegrov *et al.*, *Phys. Rev. Lett.* **85**, 1548 (2000).
- [12] W.G. Spitzer, G.A. Kleinman, and C.J. Frosch, *Phys. Rev.* **113**, 133 (1959).
- [13] W.G. Spitzer, G.A. Kleinman, and D. Walsh, *Phys. Rev.* **113**, 127 (1959).
- [14] D. Olego and M. Cardona, *Phys. Rev. B* **25**, 3889 (1982).
- [15] D. Polder and M. Van Hove, *Phys. Rev. B* **4**, 3303 (1971).
- [16] K. Joulain *et al.*, *Surf. Sci. Rep.* **57**, 59 (2005).
- [17] S. Barkeshli, *Int. J. Infrared Millim. Waves* **13**, 507 (1992).